Progress In Electromagnetics Research C, Vol. 95, 239–249, 2019

A Hepta-Band Metal-Rimmed Antenna without Lumped Elements for Smartphone Application

Peng Wang and Quanyuan Feng*

Abstract—As seen from this article, a novel hepta-band metal-rimmed antenna is proposed. The volume of the proposed antenna is small, and no lumped elements are used. The proposed metal-rimmed antenna is competitive for modern mobile application. The illustrated antenna could be divided into several parts: main ground plane, metal rim, two L-shaped ground slots sharing one open end, an L-shaped branch extended from right edge of main ground, a microstrip feedline located at the top surface of the substrate, a meandered branch located at the back side of the substrate, and a 2 mm slot located at the middle of the metal rim's top edge. For lower band, GSM850 and GSM900 are provided by two bezel loop modes generated through capacitive coupling of feedline. For upper band, DCS, PCS, UMTS, LTE2300, and LTE2500 are covered by multiple modes of two L-shaped slots, a meandered strip and feedline. With the proposed structure, the volume of the proposed antenna could be further reduced. All the mentioned operating bands are achieved in a small area of 620 mm^2 on a $115 \times 70\,mm^2$ system board. Note that the proposed antenna has achieved such a small volume on a relatively small system board without any lumped elements. The rest of this paper will describe the antenna configuration, the analysis of working principle, parametric analysis, and the experimental results are also given and discussed.

1. INTRODUCTION

Smartphones have become an essential part of our daily life. Traditionally, mobile phones are mainly used to communicate with each other. In order to improve signal intensity and to be carried easily, phones should have the characteristics of miniaturization, multiband, high gain, efficiency, etc. With the rapid development of technology, metal-rimmed antennas are designed to satisfy consumers' demand of better appearance and strength. However, when the inner antenna is surrounded by the metal rim, the inner antenna's performance degrades sharply. To improve metal-rimmed antennas' performance, designers look for various methods [1–17] to reduce the bad effect of metal rim to the inner antenna.

Combining slot antennas [1–6] and metal rim is a great way to resolve the problem due to the excellent characteristic of slot antennas. For slot antennas, the excited slot electric current mainly concentrates on the neighbor of slot and has little influence on the metal rim modes and other monopole modes of the unground portion. Hence, integrating slot antennas into metal-rimmed antenna will reduce the bad effect of the metal rim. In [5], the antenna consists of metal rim, two separate L-shaped slots etched on the main ground, and a feedline. By combining the excited loop modes, slot modes, and monopole modes, the proposed antenna achieves a wide bandwidth. However, the length of antenna portion is 10 mm, which is too large. Two slits etched on the metal rim will degrade the strength of antenna, and high band could not be covered fully. Besides, the metal rim can also be used as the portion of radiation elements [7–11]. In [9], two slits are etched on the metal rim. Several monopole branches are attached to the slit edge of the metal rim. By exciting monopole branches and coupled

Received 10 August 2019, Accepted 29 August 2019, Scheduled 16 September 2019
* Corresponding author: Quanyuan Feng (fengquanyuan@163.com).
The authors are with the Institute of Microelectronics, University of Southwest Jiaotong, Chengdu, Sichuan, China.

branches, the proposed antenna achieves hepta-band coverage. However, two slits on the metal rim will decrease the stability of the phone. Except for adjusting the radiation structure, the application of matching network [2, 4, 7, 10–14] and reconfigurable antennas [6, 18–20] is also an effective method for resolving the problem. Using lumped elements could shorten the length of radiation branches and make the height of clearance small. However, it is difficult to design and manufacture, and the lumped elements also bring extra energy loss.

In the open literature, researchers try their best to reduce the clearance size on the ends of the substrate. However, two-side clearance between rim and ground plane occupy large area. With the TCM (Theory of characteristic modes) developed, many antennas based on the TCM waste more celeriac area surrounding the ground plane. Hence, although the presented antenna has no advantage in two end clearance area, the overall occupied area is relatively small. Furthermore, when the length of the antenna is less than 120 mm, it is difficult to generate low frequency resonant points because the size of the ground plane is too small to excite low frequency current. As shown in Table 1, the volume of the proposed antenna is significantly small, and the area of the whole substrate and slot between substrate and rim is comparatively small. Furthermore, the proposed antenna does not use any lumped elements. Hence, the proposed antenna is promising for modern metal-rimmed phone.

As seen from this article, the proposed metal-rimmed antenna could cover seven bands. The proposed antenna's geometry is simple and has no lumped elements, which consists of metal rim, main ground, two L-shaped slots etched on the ground plane, L-shaped branch extended from right edge of main ground, and a meandered branch located at the back side of the substrate. By exciting multiple monopole modes, slot modes and loop modes, the proposed antenna could cover LTE/WWAN

Table 1. Performance comparison with literature.

	Volume (mm^2)	**Profile (mm)**	**Working band**	**Area Size (mm^2)**	**Lumped element**	**Eff. (%)**
[3]	876	1	Five-band	115×56.5	No	Low: > 60 High: > 60
[6]	680	0.8	Octa-band	130×74	Yes	Low: > 50 High: > 50
[7]	866.8	0.8	Hepta-band	130×70	Yes	Low: > 42 High: > 51
[9]	642.1	0.8	Hepta-band	140×70	No	Low: > 50 High: > 50
[10]	700	0.8	Octa-band	140×70	Yes	Low: > 47 High: > 43
[12]	924	0.8	Hepta-band	150×76	Yes	Low: > 41 High: > 49
[16]	1416	5	Hepta-band	126×66	No	Low: > 54 High: > 50
Prop.	**620**	**0.8**	**Hepta-band**	$\mathbf{115 \times 70}$	**No**	**Low: > 45** **High: > 41**

Five-band: GSM850, GSM900, UMTS, GSM1800, GSM1900, UMTS.

Hepta-band: GSM850, GSM900, UMTS, GSM1800, GSM1900, UMTS, LTE2300, and LTE2500.

Octa-band: LTE700, GSM850, GSM900, UMTS, GSM1800, GSM1900, UMTS, LTE2300, and LTE2500.

Efficiency: the first and second values are the lowest efficiency at the lower and higher frequency bands, respectively.

Note: The Volume include celerance area and the area between ground plane and the metal rim.

bands. Although the structure of slot is similar to the slot shape [2], the antennas' operation principles are different. The simulated results of the illustrated antenna are simulated by the electromagnetic simulation software HFSS 15.0, and the measured results are also given in the final part of this letter.

2. DESIGN CONFIGURATION AND PRINCIPLE OF OPERATION

2.1. Design Configuration

Fig. 1(a) illustrates the metal-rimmed antenna's 3D structure. The L-shaped feedline with tuning paster is located at the front side of an FR4 substrate with relative permittivity of 4.4 and loss tangent of 0.024. A pair of L-shaped slots is located at the top edge of main ground. An L-shaped branch extends from the right edge of the main ground. A meandered branch is located at the back side of the substrate with the size of 115 mm × 70 mm × 0.8 mm. The metal rim's width is 5 mm, and thickness is 0.8 mm. A 2 mm slit is etched on the top middle of the metal rim. Fig. 1(b) and Fig. 1(c) show the enlarged dimensions of the proposed antenna and the enlarged dimensions of the meandered strip, respectively. A 50 Ω SMA connector is used for feeding the metal-rimmed antenna.

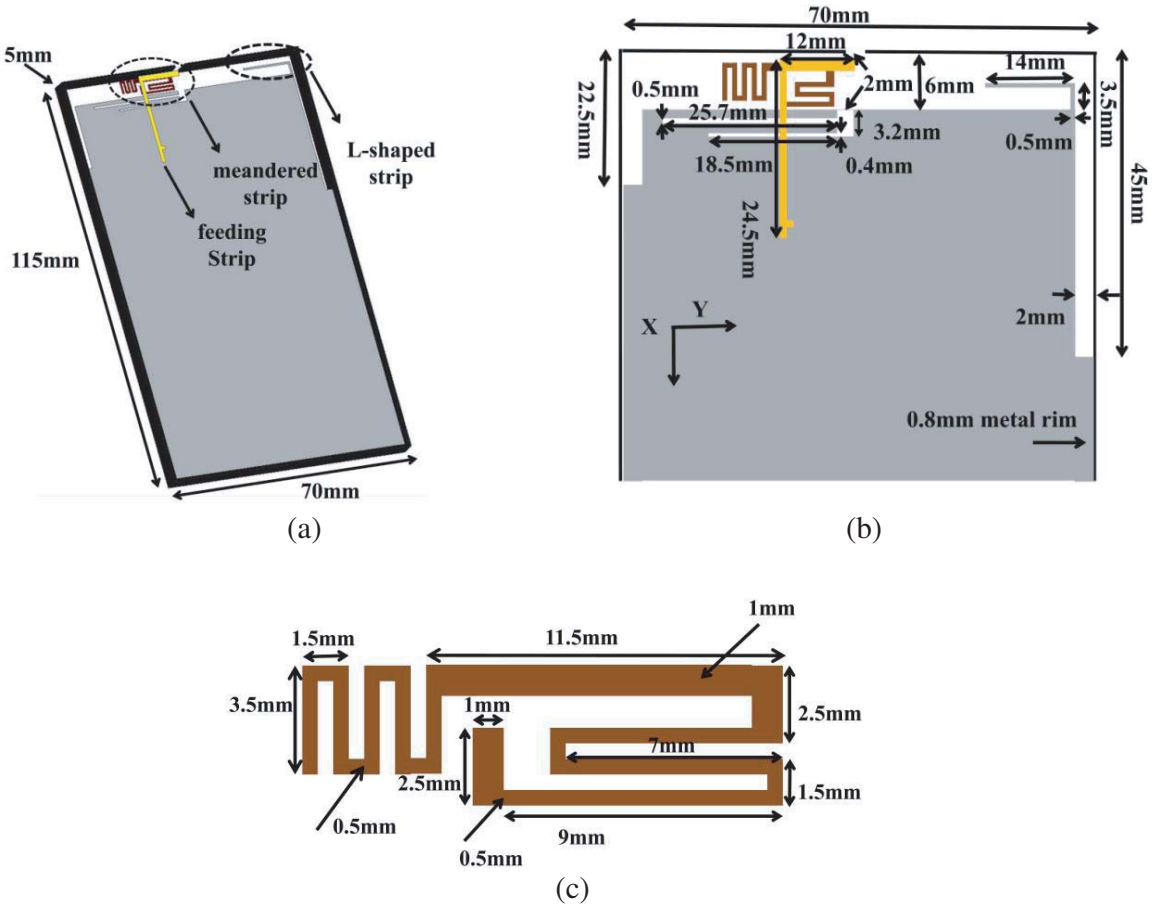

Figure 1. Proposed antenna configuration: (a) 3D structure of the metal-rimmed antenna for hepta-band smartphone applications. (b) Enlarged dimensions of the proposed antenna. (c) Enlarged dimensions of the meandered strip.

2.2. Principle of Operation

For the purpose of comprehending the operation principle of the illustrated antenna, the design process and current path of the illustrated antenna are depicted. Fig. 2 illustrates the geometries of three

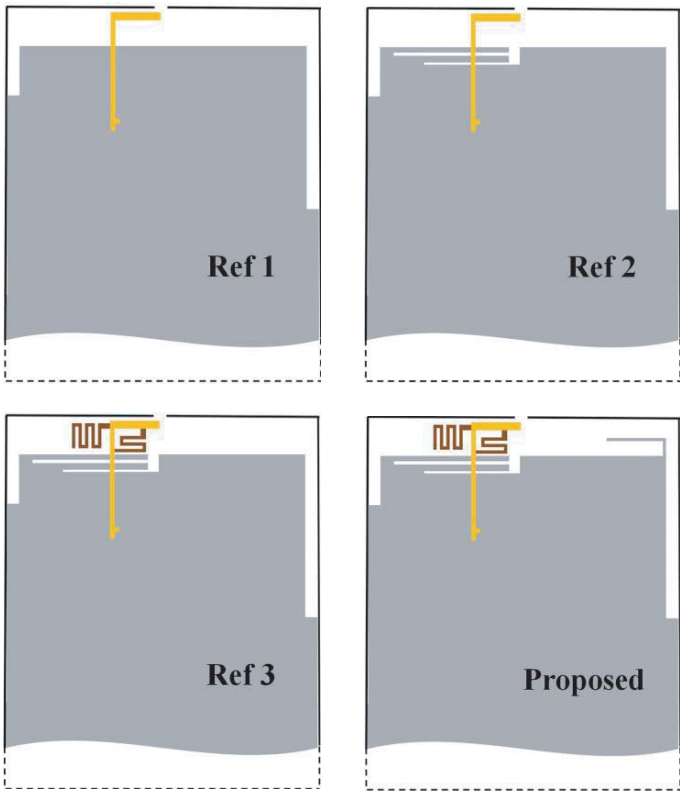

Figure 2. Structure of the reference antennas and the proposed antenna.

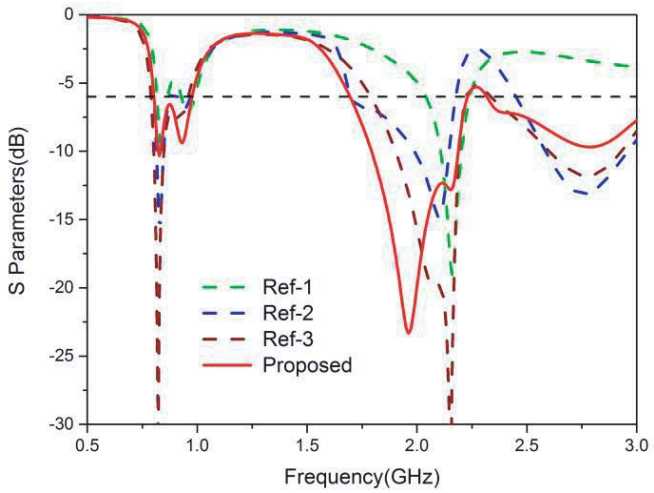

Figure 3. Simulated return loss of the three antennas and the proposed antenna.

reference antennas and the proposed antenna. Ref 1 consists of metal border, feedline, and main ground. Ref 2 adds two slits on the ground plane. In Ref 3, a meandered strip is introduced on the back side of the substrate. And the proposed antenna adds an L-shaped branch extended from the right edge of the main ground to tune the impedance matching in the high band. Fig. 3 depicts the above antennas' corresponding impedance bandwidths.

As seen from the return loss of Ref 1, there exist resonant frequency points at 840 MHz, 960 MHz, and 2160 MHz. The low band's impedance matching is bad. When two ground slots are inserted, the

return loss of Ref 2 introduces two resonant frequency points at 1740 MHz and 2760 MHz. As seen in the return loss of Ref 3, there exists a new resonant frequency point at 2330 MHz. The matching network in the low band becomes better because the introduction of meandered strip compensates the capacitance of the low frequency band. However, the frequency point around 1740 MHz shifts toward high frequency. Then, an L-shaped branch extended from the main ground is introduced to extend the current path at 1740 MHz.

We can see from the proposed antenna's impedance bandwidth, the third frequency point shifts toward low frequency.

The current distribution of each resonant mode is illustrated in Fig. 4 and Fig. 5. In order to

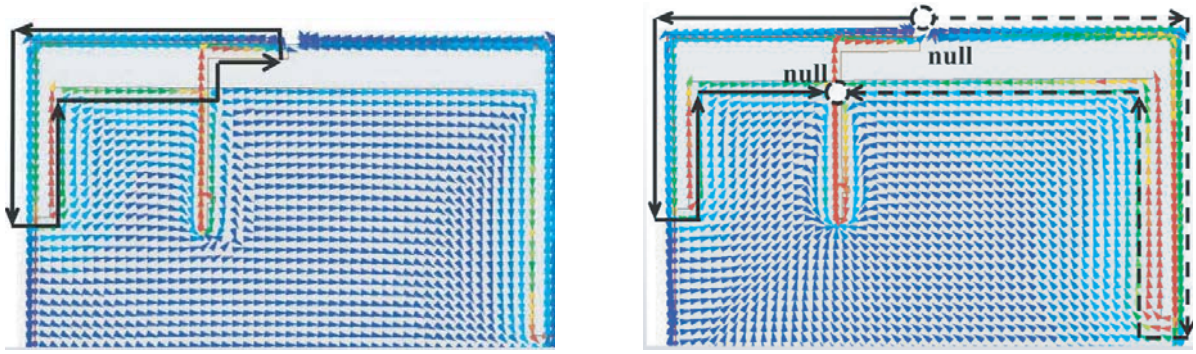

(a) (b)

Figure 4. Surface current distributions of the proposed antenna: (a) 840 MHz, (b) 960 MHz.

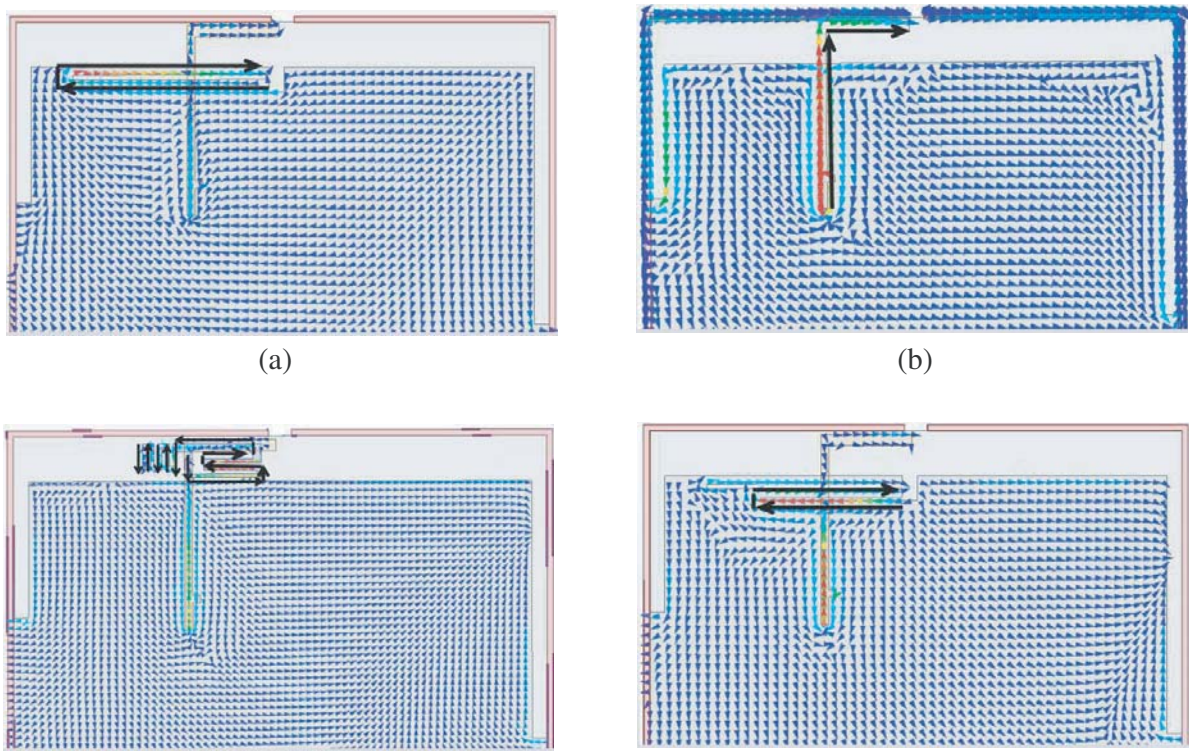

(a) (b)

(c) (d)

Figure 5. Surface current distributions of the proposed antenna: (a) 1740 MHz, (b) 2160 MHz, (c) 2330 MHz, and (d) 2760 MHz.

clearly clarify how each mode generates, we choose current distributions of Ref 1, Ref 2, and Ref 1 with a meandered strip to analyse the working principle. As seen from Fig. 4(a), the current path at 840 MHz along the left side of the metal rim with length of 114.1 mm corresponds to 0.5 λ loop mode. As seen from Fig. 4(b), the current path at 960 MHz along the loop consists of a metal rim and top edge of main ground with length of 207.5 mm corresponds to 1λ loop mode (two nulls). As seen from Fig. 5(a), the current path at 1740 MHz along the upper L-shaped slot with length of 28.7 mm corresponds to 0.25λ open slot mode. Fig. 5(b) shows the current path at 2160 MHz along the feedline with a length of 36.1 mm corresponding to 0.25λ monopole mode. Fig. 5(c) shows the current path at 2330 MHz along the meandered strip with a length of 62.5 mm corresponding to 0.25λ monopole mode. As seen from Fig. 5(d), the current path at 2760 MHz along the lower L-shaped slot with length of 23.8 mm corresponds to 0.25λ open slot mode. Due to substrate's loading effect and coupling effect of different radiation branches, the length of actual current path is shorter than the theoretical length. However, the length of the current path at 2330 MHz is longer than the theoretical length because current mainly concentrates on the horizontal distributed inductance.

3. PARAMETRIC ANALYSIS

3.1. Effect of Rim Slot and L-Shaped Strip

The effect of the location of the rim slot and the vertical length of inverted L-shaped strip extended from the ground plane are shown in Fig. 5. As shown in Fig. 6(b), with the increase of $L1$, the frequency point around 1.7 GHz moves to lower frequency. Meanwhile, the frequency point near 960 MHz shifts toward high frequency, and the impedance matching in GSM850/GSM900/DCS/PCS/UMTS bands becomes

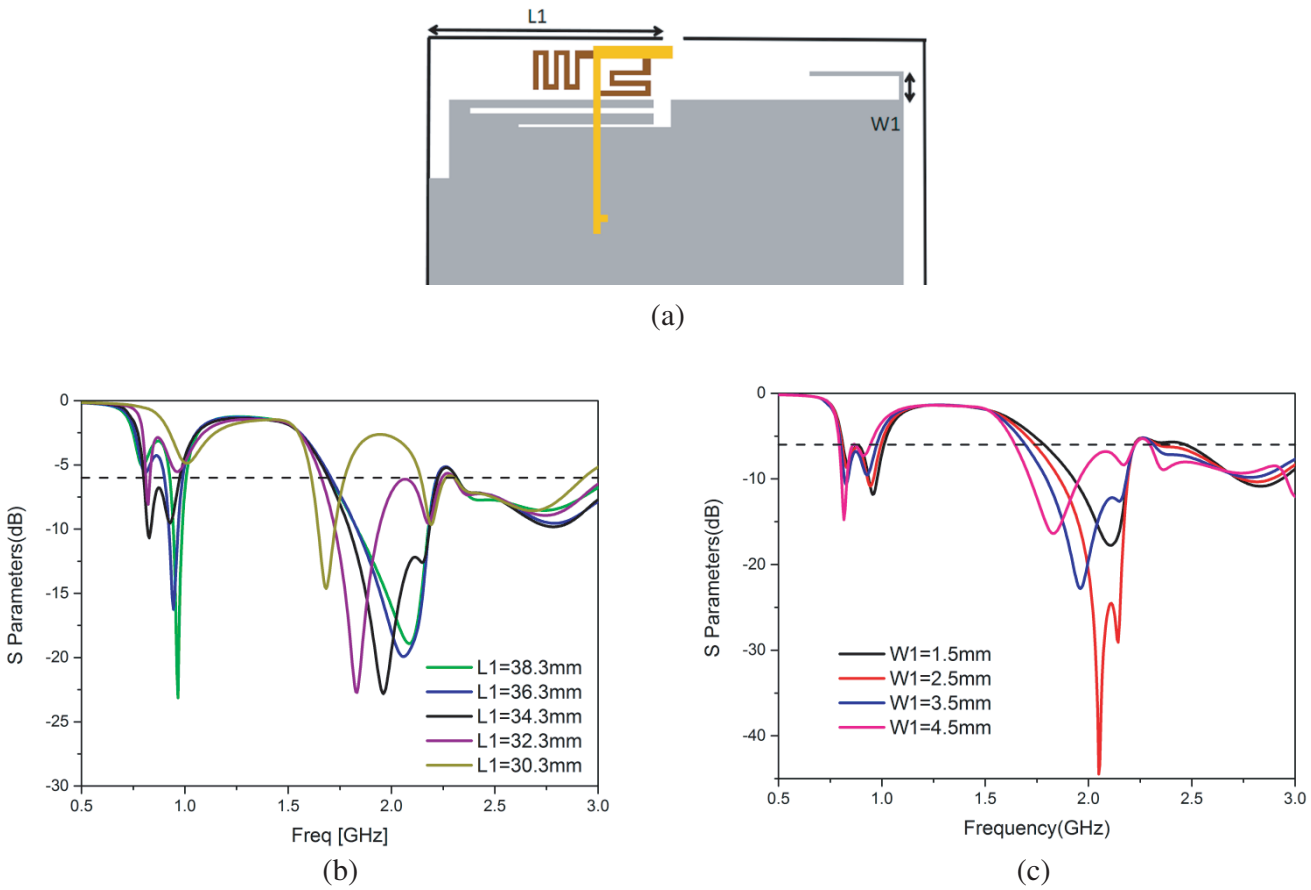

Figure 6. Simulated return loss for (a) the antenna element as a function of (b) $L1$, (c) $W1$.

worse. As shown in Fig. 6(c), with the increase of $W1$, the frequency point around 1.7 GHz and 960 MHz shifts toward lower frequency, and impedance matching in LTE2300/LTE2500 bands becomes better.

4. EXPERIMENTAL RESULTS AND DISCUSSION

4.1. Free Space

We measure the return loss and far-field parameters by the Agilent N5247A vector network measurement instrument and SATIMO measurement system SG24-C, respectively. Fig. 7, Fig. 8, and Fig. 9 show the measured planar radiation patterns at 900 MHz, 1900 MHz, and 2500 MHz. For the low frequency, 0.5λ dipole omnidirectional radiation pattern is illustrated in the XZ-plane at 900 MHz. For the high band, the figures of $E\varphi$ and $E\theta$ show good complementary characteristic. The far-field radiation characteristic is acceptable for ensuring the communication quality. Fig. 10 shows pictures of the manufactured protype and test scenario. Fig. 11 illustrates the simulated and measured impedance bandwidths of the illustrated antenna. The tested and measured return losses show good consistency. The simulated and measured impedance bandwidths can cover LTE/WWAN bands for smartphone application. Fig. 12 and Fig. 13 depict the tested far-field radiation characteristic. In the lower band, the gain varies between 0.8 dBi and 1.15 dBi, and the efficiency ranges from 45% to 58%. In the higher band, the gain ranges

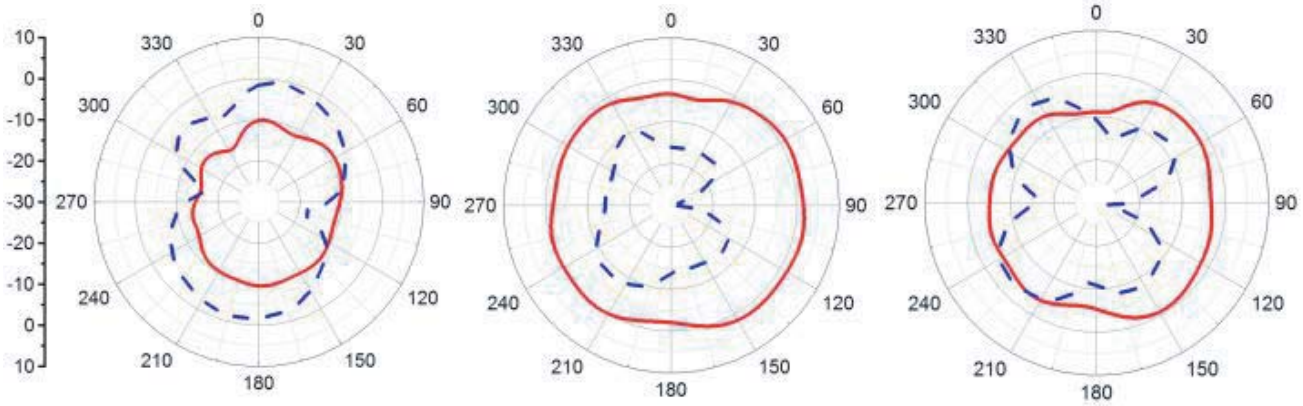

Figure 7. Measured xz-plane radiation patterns of the proposed antenna (red line is $E\theta$, blue line is $E\varphi$, unit: dBi) at three principal planes. (a) 900 MHz, (b) 1900 MHz, (c) 2500 MHz.

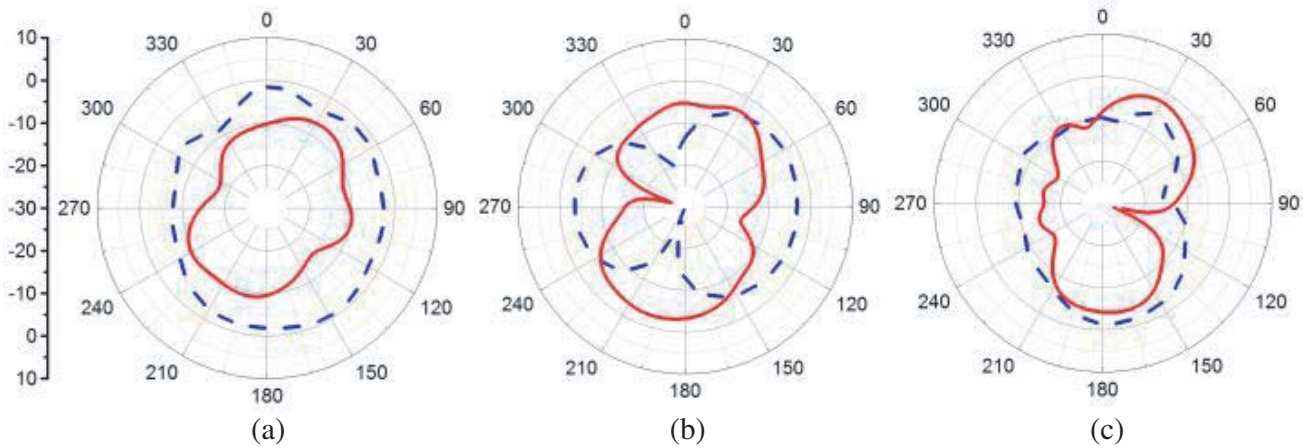

Figure 8. Measured yz-plane radiation patterns of the proposed antenna (red line is $E\theta$, blue line is $E\varphi$, unit: dBi) at three principal planes. (a) 900 MHz, (b) 1900 MHz, (c) 2500 MHz.

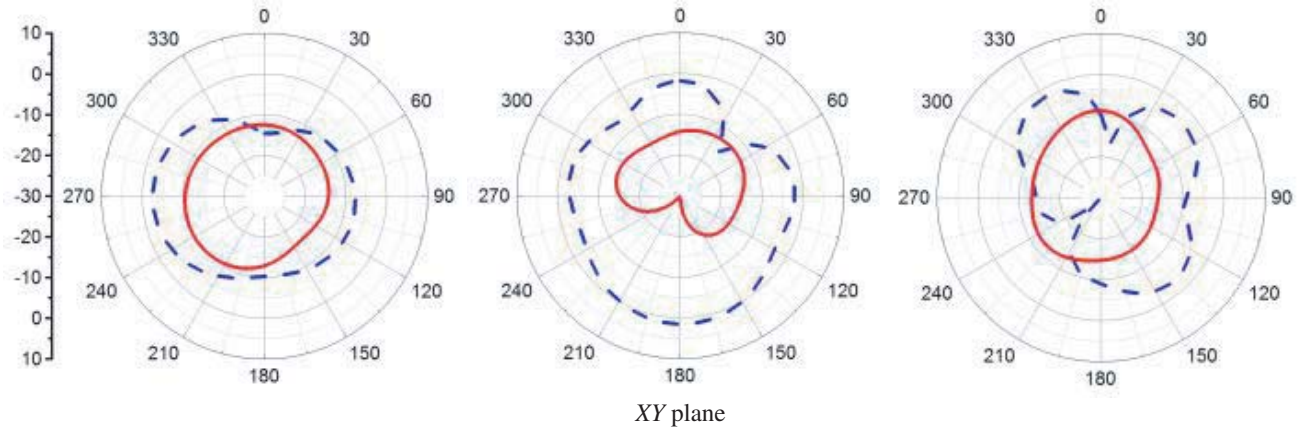

Figure 9. Measured xy-plane radiation patterns of the proposed antenna (red line is $E\theta$, blue line is $E\varphi$, unit: dBi) at three principal planes. (a) 900 MHz, (b) 1900 MHz, (c) 2500 MHz.

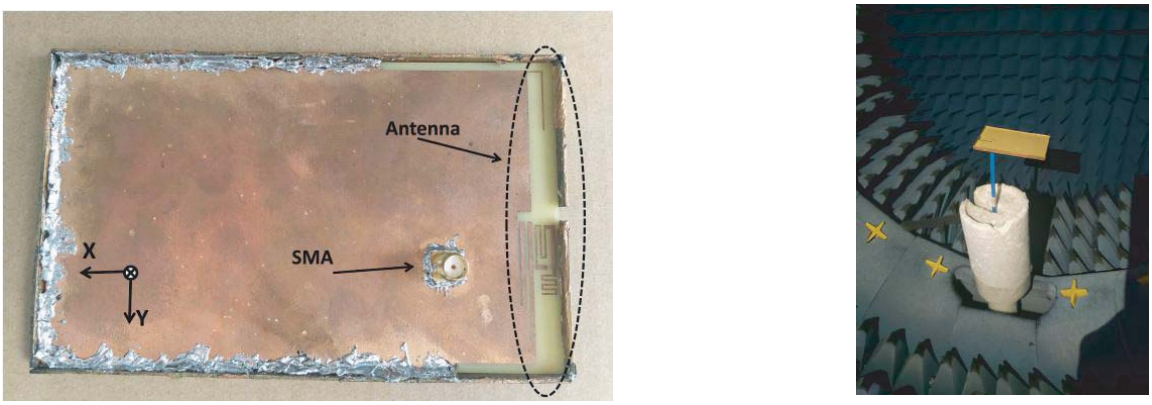

Figure 10. The photograph of the fabricated protype and test scenario.

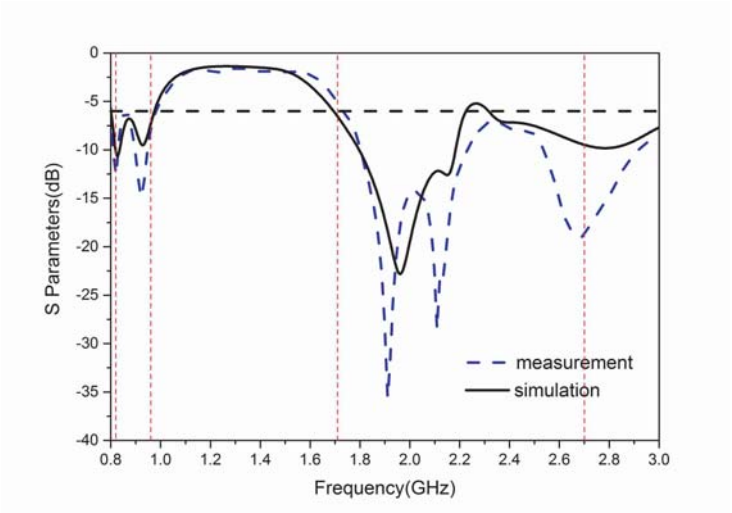

Figure 11. Simulated and measured return losses of the proposed antenna.

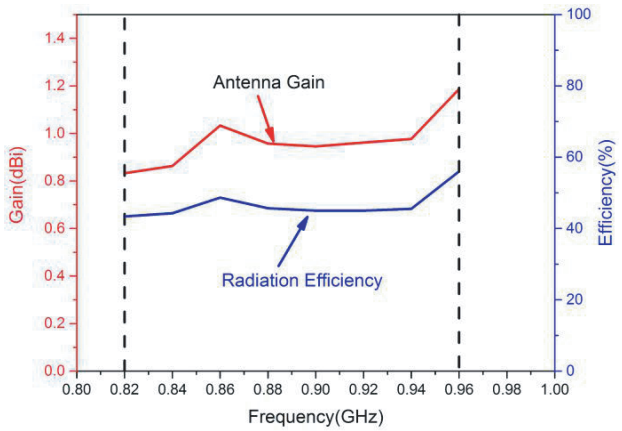

Figure 12. Measured gain and efficiency in the lower band.

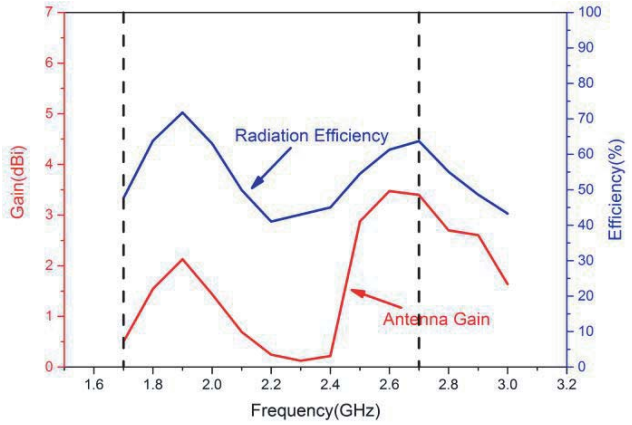

Figure 13. Measured gain and efficiency in the higher band.

from 0.2 dBi to 3.5 dBi, and the efficiency ranges from 41% to 75%. The measured results indicate that the proposed metal-rimmed antenna is competitive for future mobile application.

4.2. Hand's Effect

Figure 14 shows the tested impedance bandwidth when hand grips at different positions of the handset. The top position represents the area where the antenna occupies. The middle position represents the middle portion of the antenna. The bottom position represents the portion where the antenna does not exist. The return losses of middle position and bottom position have little difference. However, when

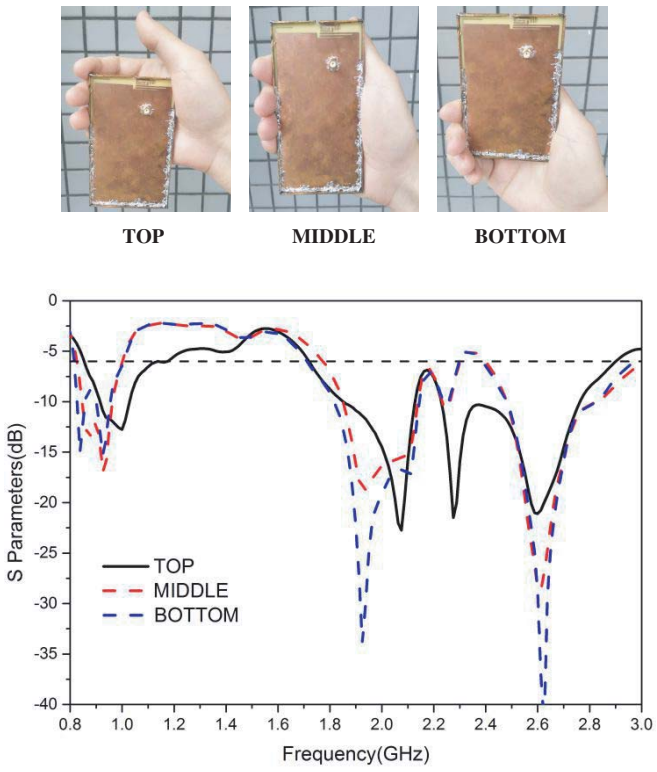

Figure 14. Measured return loss of different grip position.

the hand grips at top position, the impedance bandwidth changes greatly especially in the low band because the hand absorbs a portion of radiation energy. It will result in the reduction of Q-factor, and the bandwidth will be broadened.

5. CONCLUSION

A novel hepta-band metal-rimmed antenna for smartphone application is presented. The proposed antenna has a simple structure and does not use lumped elements. The antenna consists of a metal rim, a feedline, a main ground, L-shaped slots on the ground plane, a meandered strip on the bottom of the substrate, and an L-shaped branch located at the right edge of the main ground. The L-shaped branch is utilized for tuning the impedance matching of the high band and low band. By exciting multiple modes and tuning the impedance matching, the metal-rimmed antenna could cover LTE/WWAN bands. The measured results indicate that the proposed antenna could be applied to metal-rimmed smartphone application.

ACKNOWLEDGMENT

This work is supported by Key Project of the National Natural Science Foundation of China under Grant 61531016, 61831017 and the Sichuan Provincial Science and Technology Important Projects under Grant: 2018GZ0139, 2018GZDZX0001

REFERENCES

1. Hsu, C. K. and S. J. Chung, "Single open-slot antenna for LTE/WWAN smartphone application," *IEEE Trans. Antennas Propag.*, Vol. 63, No. 11, 5102–5107, Nov. 2017.
2. Wong, K. L. and C. Y. Huang, "Triple-wideband open-slot antenna for the LTE metal-framed tablet device," *IEEE Trans. Antennas Propag.*, Vol. 63, No. 12, 5966–5971, Dec. 2015.
3. Yuan, B., Y. Cao, G. Wang, et al., "Slot antenna for metal-rimmed mobile handsets," *IEEE Antennas Wireless Propag. Lett.*, Vol. 11, 1334–1337, 2012.
4. Wong, K. L. and C. Y. Tsai, "Low-profile dual-wideband inverted-T open slot antenna for the LTE/WWAN tablet computer with a metallic frame," *IEEE Trans. Antennas Propag.*, Vol. 63, No. 7, 2879–2886, Jul. 2015.
5. Ban, Y. L., Y. L. Yang, M. Y. Li, et al., "Printed monopole slot antenna for WWAN metal-rimmed smartphone applications," *The Int. Symp. Antennas Propag. (ISAP)*, 2015.
6. Stanley, M., Y. Huang, H. Wang, et al., "A novel reconfigurable metal rim integrated open slot antenna for octa-band smartphone applications," *IEEE Trans. Antennas Propag.*, Vol. 65, No. 7, 3352–3363, Jul. 2017.
7. Zhang, L. W., Y. L. Ban, C. Y. D. Sim, et al., "Parallel dual-loop antenna for WWAN/LTE metal-rimmed smartphone," *IEEE Trans. Antennas Propag.*, Vol. 66, No. 3, 1217–1226, Mar. 2018.
8. Huang, D., Z. Du, and Y. Wang, "An octa-band monopole antenna with a small nonground portion height for LTE/WLAN mobile phones," *IEEE Trans. Antennas Propag.*, Vol. 65, No. 2, 878–882, Feb. 2017.
9. Liu, Y., Y. Zhou, G. Liu, et al., "Hepta-band inverted-F antenna for metal-rimmed mobile phone applications," *IEEE Antennas Wireless Propag. Lett.*, Vol. 15, 996–999, 2016.
10. Chen, H. and A. Zhao, "LTE antenna design for mobile phone with metal frame," *IEEE Antennas Wireless Propag. Lett.*, Vol. 15, 996–999, 2016.
11. Liu, G., Y. Liu, and S. Gong, "A coupled-fed loop antenna for metal-rimmed mobile phone applications," *Microw. Opt. Technol. Lett.*, Vol. 59, No. 2, 311–314, Feb. 2017.
12. Xu, Z., Q. Q. Zhou, Y. L. Ban, et al., "Hepta-band coupled-fed loop antenna for LTE/WWAN unbroken metal-rimmed smartphone applications," *IEEE Antennas Wireless Propag. Lett.*, Vol. 17, No. 2, 311–314, 2018.

13. Kuixi, Y., Y. Peng, Y. Feng, et al., "Antenna design for a smartphone with a full metal casing and a narrow frame," *IET Microw., Antennas Propag.*, Vol. 12, 1316–1323, Jun. 2018.
14. Huang, D. and Z. Du, "Eight-band antenna with a small ground clearance for LTE metal-frame mobile phone applications," *IEEE Antennas Wireless Propag. Lett.*, Vol. 17, 34–37, 2018.
15. Lian, J. W. and Y. L. Ban, "Hybrid multi-mode narrow-frame antenna for WWAN/LTE metal-rimmed smartphone applications," *IEEE Access*, Vol. 4, 3991–3998, 2016.
16. Yang, Y., Z. Zhao, W. Yang, et al., "Compact multimode monopole antenna for metal-rimmed mobile phones," *IEEE Trans. Antennas Propag.*, Vol. 65, No. 5, 2297–2304, May 2017.
17. Chen, S. C., C. C. Huang, and W. S. Cai, "Integration of a low-profile, long-term evolution/wireless wide area network monopole antenna into the metal frame of tablet computers," *IEEE Trans. Antennas Propag.*, Vol. 65, No. 7, 3726–3731, Jul. 2017.
18. Ban, Y. L., Y. F. Qiang, G. Wu, Y. L. Ban, et al., "Reconfigurable narrow-frame antenna for LTE/WWAN metal-rimmed smartphone applications," *IET Microw., Antennas Propag.*, Vol. 10, No. 10, 1092–1100, Jul. 2016.
19. Zhang, H. B., Y. L. Ban, Y. F. Qiang, et al., "Reconfigurable loop antenna with two parasitic grounded strips for WWAN/LTE unbroken-metal-rimmed smartphones," *IEEE Access*, Vol. 5, 4840–4845, 2017.
20. Xu, Z. Q., Y. T. Sun, Q. Q. Zhou, et al., "Reconfigurable MIMO antenna for integrated-metal-rimmed smartphone applications," *IEEE Access*, Vol. 5, 21223–21228, 2017.